Kyushu University Global COE Program
Journal of Novel Carbon Resource Sciences, Vol. 7, pp. 12-17, Feb. 2013

Rise and Dissolution Modeling of CO_2 Droplet in the Ocean

Changhong Hu[*1,*2], Makoto Sueyoshi[*1,*2], Fei Jiang[*3],
Kiminori Shitashima[*2], Tetsuo Yanagi[*1,*2]

[*1] Research Institute for Applied Mechanics, Kyushu University
[*2] International Institute for Carbon-Neutral Energy Research (WPI- I2CNER), Kyushu University
[*3] Interdisciplinary Graduate School of Engineering Science, Kyushu University

(Received October 26, 2012; accepted December 12, 2012)

A numerical approach is proposed to study the behavior of a natural carbon dioxide (CO_2) droplet leaked from the seafloor. Motion and deformation of the droplet at the initial stage are simulated by a lattice Boltzmann multi-phase method to obtain the terminal velocity. The whole process of droplet rise and dissolution is modeled by a simplified analytical method. The in-situ experiment case on a natural CO_2 droplet at the Okinawa Trough (Shitashima, et al.[1]) is studied by using the proposed numerical model. Numerical experiments show strong dependency between the terminal velocity and the droplet density. The phenomena obtained in the on-sea observation are discussed by the present numerical study.

1. Introduction

The ocean based carbon capture and storage (CCS) technology is considered as a hopeful method to mitigate the global warming. Among several types of the ocean CCS, the ocean geological CCS, in which the CO_2 is stored beneath the seabed, will be the most practicable approach in the near future. However, due to unpredictable reasons such as earthquake, there is still a risk of CO_2 leakage from the storage reservoir. It is necessary to investigate the behavior of rising CO_2 droplets for elucidation of the impact on marine ecosystems and for designing an efficient monitoring system.

One approach to study CO_2 droplet in the deep sea is the natural analogue. Large amount of natural CO_2 oozes from the seabed around under-sea volcanoes. Observation of this kind of CO_2 droplet provides an opportunity for understanding the behavior of CO_2 in the ocean. Shitashima et al.[1] carried out a series of in-situ experiments on rising hydrothermal CO_2 droplets from 1430 m deep seafloor at the Okinawa Trough. They tracked the CO_2 droplets emitted from the seafloor by a remotely operated vehicle (ROV) for several hundred meters. In-situ data of temperature, salinity, pH and partial pressure of CO_2 (pCO_2) near the CO_2 droplets were measured, and the change in droplet size and rise rate were also calculated from the video record. For droplet with about 7 mm diameter, the average rise rate is about 20 cm/s. On the other hand, P. G. Brewer et al.[2] performed a real sea in-situ experiment in 800 m deep Monterey Bay, California. They released pure CO_2 droplets by a pipe and tracked them by a ROV. However, the mean ascent rate measured in the experiment is 12.8 cm/s for the droplet with the similar size of Shitashima's experiment. The motivation of the present research is to find out the reason of this discrepancy.

Since in-situ experiment in the deep ocean usually encounters difficulties such as riskiness and high cost, the numerical simulation is considered as an efficient method which can provide much more detailed information. Recently, a novel lattice Boltzmann method (LBM or LB method) has been developed by Jiang and Hu[3] for this purpose. LBM has several advantages over the conventional Navier-Stokes solver, especially in dealing with complex boundaries, incorporating of microscopic interactions, and parallelization of the algorithm. The liquid CO_2 and seawater system is a typical immiscible multi-phase flows problem and can be treated by the LBM with the Rothman-Keller/ Gunstensen (RK) two-phase model. The initial stage of a CO_2 droplet rising, i.e., the droplet moves from quiescence to steady state at the terminal velocity, is simulated by the LBM. Deformation of the droplet is an important factor of this stage. Simulation of the whole process of the droplet rising until it is fully dissolved in the seawater will cost too much CPU time by LBM. Therefore, a simplified analytical method is also proposed in this paper to model the whole process of the droplet rise with the consideration of dissolution.

This paper is organized as follows. In section 2, the RK multi-phase LBM model are briefly introduced with validations. In section 3, the simplified analytical model is proposed. In section 4, Shitashima's in-situ experiment case is studied by the proposed numerical model. Finally, a conclusion of this study is described.

2. Lattice Boltzmann two-phase model

In this section the lattice Boltzmann two-phase RK model is outlined. A D3Q19 (nineteen velocity vectors in 3D) lattice model is adopted in this study. This method includes two LB schemes: a LB flow solver with the multi-relaxation time (MRT) collision operator[4] incorporating the effects of surface tension, and a LB scheme for the phase field[5].

2.1 Lattice Boltzmann scheme for flow field

The lattice Boltzmann equation to describe fluid flows can be as

$$f_i(\mathbf{x}+\mathbf{c}_i\delta t, t+\delta t) = f_i(\mathbf{x},t)+\Omega_i, \qquad i=0,\cdots 18. \quad (1)$$

In the equation, $f_i(\mathbf{x},t)$ is the particle distribution function which represents the probability of finding a particle at the node **x** and the time t with velocity $\mathbf{c}_i$. δt is the time step relating to the grid spacing through $h = c\cdot\delta t$. The collision operator of the MRT model is given by

$$\mathbf{\Omega} = \mathbf{M}^{-1}\mathbf{S}\left[(\mathbf{Mf}) - \mathbf{m}^{eq}\right], \quad (2)$$

where M is the transformation matrix[6]. This matrix is constructed from the orthogonal basis vectors[7], which transforms the distributions into moment space. The equilibrium vector $\mathbf{m}^{eq}$ is composed of equilibrium moments[7]. During the collision, the moments $\{m_k$, k = 0, 3, 5, 7$\}$ are always conserved, leading to mass and momentum conservation of this algorithm. The matrix **S** is a diagonal collision matrix indicating the relaxation rates. The collision parameters $S_{i,i}$ (the eigenvalues of the collision matrix) contain zero parts and non-zero parts. The non-zero parts are

$$\begin{aligned}
&s_{1,1} = -s_e,\\
&s_{2,2} = -s_\xi,\\
&s_{4,4} = s_{6,6} = s_{8,8} = -s_q,\\
&s_{10,10} = s_{12,12} = -s_\pi,\\
&s_{9,9} = s_{11,11} = s_{13,13} = s_{14,14} = s_{15,15} = -s_\nu,\\
&s_{16,16} = s_{17,17} = s_{18,18} = -s_m.
\end{aligned} \quad (3)$$

The relaxation rate s_ν can be calculated from the kinematic viscosity ν by

$$\frac{1}{s_\nu} = 3\frac{\nu}{c^2\delta t} + \frac{1}{2}. \quad (4)$$

The parameters s_e , s_ξ , s_q , s_π and s_m have to be chosen in the range [0,2] and are used to improve numerical accuracy and stability[8].

The macroscopic properties of density variation, velocity and pressure variation are defined in terms of particle distribution function by

$$\delta\rho = \sum_{i=0}^{18} f_i, \quad \mathbf{u} = \frac{1}{\rho_0}\sum_{i=0}^{18} f_i\cdot\mathbf{c}_i, \quad \delta P = \frac{\delta\rho}{3}. \quad (5)$$

2.2 Lattice Boltzmann scheme for phase field

The advection of the phase field is also done in the LB framework and a recoloring approach[9] is implemented to keep the interface sharp. For the phase field, we introduce binary immiscible red and blue fluids with fluid density ρ_r and ρ_b, respectively. The advection of these scalar phase fields ψ, where $\psi = \rho_r$ or ρ_b, is done with a separated LB equation:

$$g_i(t+\Delta t, x+\boldsymbol{e}_i\Delta t) = g_i^{eq}(\psi(t,x),\boldsymbol{u}(t,x)). \quad (6)$$

where g_i are dimensionless density distributions. The equilibrium distribution function is given by

$$g_i^{eq}(\psi,\boldsymbol{u}) = w_i\psi\left(1+\frac{3}{c^2}\boldsymbol{e}_i\cdot\boldsymbol{u}\right). \quad (7)$$

The velocity $\boldsymbol{u}$ is computed by the flow solver described above. The weight coefficients are

$$w_i = \begin{cases} 1/3 & i=0\\ 1/18 & i=1,\cdots,6\\ 1/36 & i=7,\cdots,18\end{cases}. \quad (8)$$

An order parameter ϕ is then defined as

$$\phi = \frac{\rho_r-\rho_b}{\rho_r+\rho_b}. \quad (9)$$

Here $\phi = 1$ means the red phase and $\phi = -1$ means the blue phase. The value of ϕ is constant in the bulk of each phase and varies in the range [-1,1] at the diffusive interface. Then the gradient of the phase field **C** is defined and can be calculated using this order parameter:

$$\mathbf{C}(t,x) = \frac{3}{c^2\Delta t}\sum_i w_i\,\boldsymbol{e}_i\phi(t,x+\boldsymbol{e}_i\Delta t). \quad (10)$$

The normalized gradient, which defines the orientation of the interface, is obtained by

$$n_\alpha = \frac{\mathrm{C}_\alpha}{|\mathbf{C}|}. \quad (11)$$

The color gradient **C** introduced in the phase field solver is used to calculate additional terms which are incorporated into the equilibrium distribution functions of the moment space. These terms are applied to generate surface tension through a perturbation based on the gradient of the phase field.

This LB scheme for the phase field results in an advection diffusion equation solver[10]. The diffusion coefficient is $\alpha = (1/6)c^2\delta t$ which is undesirable for immiscible fluids and a recoloring algorithm[9] is applied to cancel out the diffusion effect. By this recoloring step, we can achieve a phase separation. The recoloring step redistributes the mass distributions of phase ρ_r and ρ_b so that the inner product of the gradient **C** and the momentum of phase ρ_r is maximized.

2.3 Validation of LBM

The above described LBM is validated against the experimental data by Ozaki[11]. In the experiment, a nozzle was used to generate various sizes of liquid CO_2 droplets in a large high-pressure tank and the terminal velocity of the droplets was measured. The experiments

were executed under the conditions with the pressure of 200 atm and the temperature of 5 °C which correspond to the situations of 2000 m deep ocean. The physical properties of the liquid CO_2/sea water system such as density, viscosity and surface tension at these conditions are listed in Table 1.

The process of CO_2 droplets with different diameters (2.0 mm - 16.0 mm) rising from quiescence to a steady state is simulated by using the above parameters. The terminal velocity of the rising droplet is calculated from the simulation result. A comparison between the numerical results and Ozaki's experiment data is shown in Fig. 1. The simulation results are in an excellent agreement with the experimental data, especially for small droplets. For the droplets with diameters below 8 mm, the spherical shape is maintained. Obvious deformations start to be observed when the droplet diameters exceed 12 mm. A nonlinear relationship between droplet size and rising velocity is found when the droplet size is larger than 10 mm.

The shapes of the droplet with diameter 14 mm at different times (t = 0.13, 0.52, 1.01 and 1.40) during rising process are shown in Fig. 2. It can be found that the droplet begins to deform soon after releasing, and becomes elliptical finally. About one second is required for these droplets to reach their terminal rising state.

The vertical computation domain is about one meter for this initial stage and the LBM simulation seems efficient and accurate. For the whole rising process which may cover several hundred meters vertical distance, the analytical model can be used.

Table 1 Physical properties of the liquid CO_2/sea water system at 5 °C, 200 atm

Property	Sea Water	Liquid CO_2
Density [kg/m^3]	1036	1010
Viscosity [kg/(ms)]	$1.6*10^{-3}$	$0.156*10^{-3}$
Interfacial tension [N/m]	$7.0*10^{-2}$	

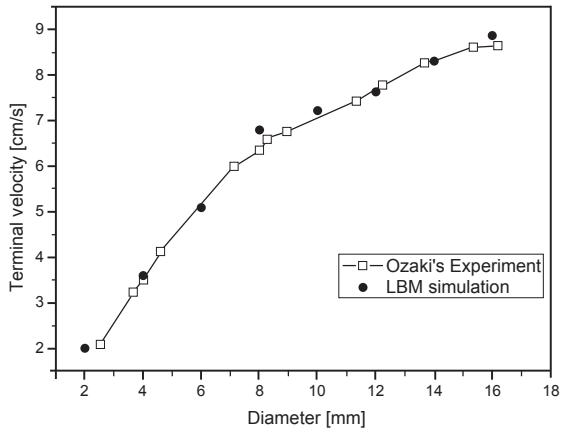

Fig. 1 Correlation between terminal velocity and droplet size.

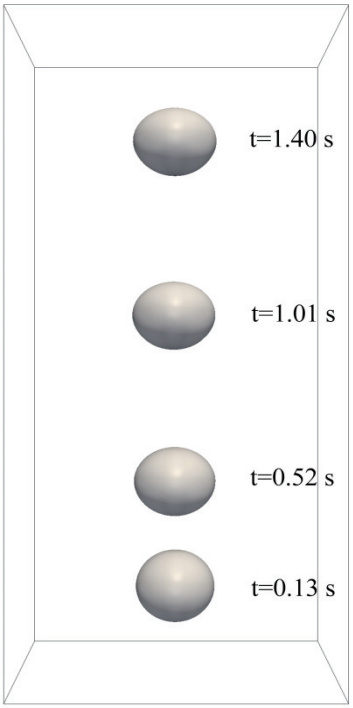

Fig. 2 Deformation of a CO_2 droplet with diameters of 14 mm.

3. Modeling droplet rise and dissolution

In this section a simplified analytical model to simulate whole the rising process of the CO_2 droplet with the consideration of dissolution is described. The motion of equation of a droplet is written as

$$\frac{d}{dt}\left(m\frac{dz}{dt}\right) = -F_d + F_b - F_g, \tag{12}$$

where m is the mass of droplet, z is the position, F_d is drag, F_b is buoyancy and F_g is gravity force. This motion of equation is numerically calculated from the initial position to the fully dissolved position explicitly. The drag force F_d is calculated by

$$F_d = \frac{1}{2}C_d\rho_s AU|U|, \tag{13}$$

where C_d, ρ_s, A and U are the drag coefficient, the density of sea water, the reference area of droplet and the rise rate at the position z, respectively. The buoyancy force F_b is calculated by

$$F_b = \rho_s Vg, \tag{14}$$

where V is the volume of droplet and g is the gravity acceleration. The gravity force F_g is expressed by

$$F_g = \rho_d Vg, \tag{15}$$

where ρ_d is the density of droplet. At each time step, the

mass of droplet is decreased by dissolution to the sea water. Variation of mass due to dissolution is given by

$$\frac{dm}{dt} = -KS\,, \tag{16}$$

where K is the dissolution rate and S is the surface area of droplet. In this model, the shape of droplet is regarded as a sphere. With the droplet density at the position z, the mass of droplet m is determined by using the reference area A and the surface area S of droplet as follows:

$$V = \frac{m}{\rho_d}, r = \left(\frac{3}{4\pi}V\right)^{\frac{1}{3}}, A = \pi r^2, S = 4A\,. \tag{17}$$

When the density of position z is given, the equation (12) is easily computed in time domain sequentially from the release position and other initial conditions. Fig. 3 shows the diagram of the numerical computation.

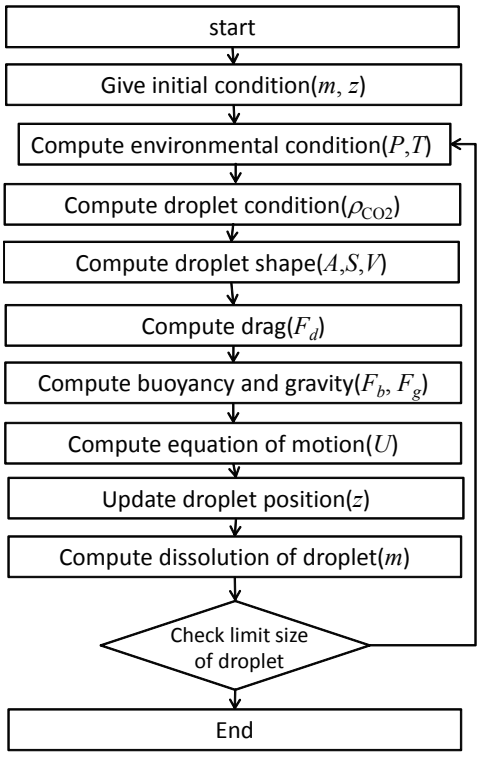

Fig. 3 Sequence diagram of numerical simulation for droplet rising by using analytical model.

4. On the in-situ experiment case

In this section, we study an in-situ experiment case[1] by the above proposed model. In the experiment, rise of hydrothermal CO_2 droplets was observed and measured. Fig. 4 shows variation of the size (projected area) and the rising rate of a CO_2 droplet in the deep sea for two cases. Observation was carried out from the seafloor at the Okinawa Trough of 1430 m depth. In general, the rise rate decreased with the increase of droplet ascent distance. It is considered that the start velocity in Fig. 4 is approximately equal to the terminal velocity. The decrease of the rising velocity is due to the reduction in the droplet size caused by the CO_2 dissolution. The start velocity, i.e., the terminal velocity, is near 20 cm/s in the measurements. In another in-situ experiment[2] by using pure liquid CO_2 droplet in the deep sea with the depth of 800 m, a mean ascent rate of 12.8 cm/s was obtained for the similar size droplet. We consider that the different depth is not the only reason which causes such large discrepancy between the two experiments. Other factors that affect the droplet rising rate need to investigate. Here we use the proposed numerical model to study this problem and try to find an answer.

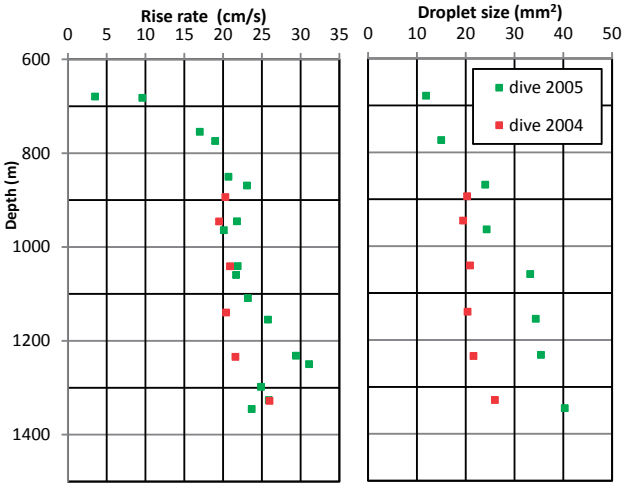

Fig. 4 Vertical change in droplet size and rise rate of CO_2 droplets.

4.1 Terminal velocity obtained by LBM

At first we check the terminal velocity at the experiment condition by numerical simulations. The LB method proposed in Section 2 is used. Physical properties of the liquid CO_2 vary with the pressure and temperature. High pressure and low temperature are the vital conditions that influence not only the density difference between sea water and liquid CO_2 but also the existence of the hydrate film on the surface of the droplet, and consequently influence the buoyance and the surface tension. In the LB method, these conditions are adjusted by changing the surface tension coefficient parameter σ and the densities of liquid CO_2 and seawater.

Numerical simulations on the two in-situ experiment cases, Shitashima's experiment[1] and Brewer's experiment[2] are carried out. The parameters used in the computation are listed in Table 2 and Table 3, respectively. Single sphere droplet with diameter of 9 mm is simulated from quiescence to steady rising status.

The terminal velocity of the droplet is computed when the droplet reaches a steady state for the above two experimental cases. For Brewer's case, the terminal velocity of 12.3 cm/s is obtained, which is very close to the experiment. Since in the experiment pure liquid

Table 2 Physical properties of the liquid CO_2/sea water system at 3.9 °C, 140 atm

Property	Sea Water	Liquid CO_2
Density [kg/m^3]	1034.9	996
Viscosity [kg/(ms)]	$1.6*10^{-3}$	$0.128*10^{-3}$
Interfacial tension [N/m]	$7.0*10^{-2}$	

Table 3 Physical properties of the liquid CO_2/sea water system at 4.4 °C, 80 atm

Property	Sea Water	Liquid CO_2
Density[kg/m^3]	1031.5	962
Viscosity[kg/(ms)]	$1.6*10^{-3}$	$0.11*10^{-3}$
Interfacial tension[N/m]	$7.0*10^{-2}$	

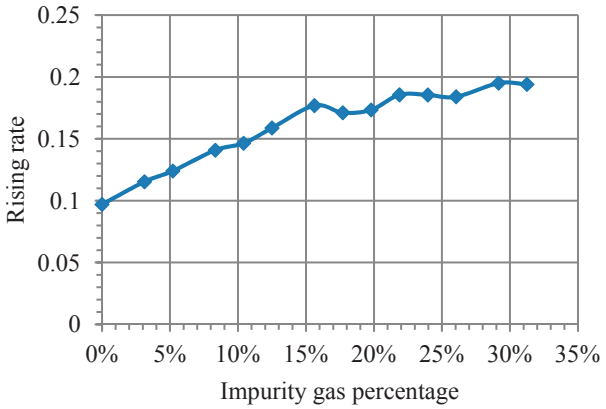

Fig. 5 Relationship between gas percentage and rising rate for a CO_2 droplet with diameter 7 mm.

CO_2 droplet is used, and the environment conditions are relatively ideal, comparison between the numerical result and the experimental result is satisfactory. On the other hand, for Shitashima's case, the calculated terminal rising rate is 9.7 cm/s, which is very below the experimental result of 20 cm/s. Several reasons can be considered for this discrepancy. First, the CO_2 droplet emitted from the seafloor near under-sea volcanoes usually contains other gas species such as methane and helium. These gas species reduce the overall density of droplet. Therefore, such large density difference can cause higher rising rate due to the larger buoyancy. In the paper[1], it is reported that the natural CO_2 droplet consists of about 5% impurities. However, as this value is obtained according to the measurement on the ground, the gas component in the droplet may be underestimated due to the environment change. The exact component of the natural CO_2 droplet in the deep ocean is impossible to measure in situ. Therefore in this study, we use numerical simulation method to investigate the effect of the purity of the CO_2 droplet on the rising velocity. The upwelling current in the deep ocean is considered as another reason which can accelerate the droplet rising rate. Since the intensity of upwelling current is very difficult to measure in the experiment and its effect on the rising velocity is considered less important than the previous reason, quantitative assessment of the upwelling current effect is left for the future research.

Therefore, in order to investigate the effect of purity on rising rate, we carried out several simulations with various densities of CO_2 droplet. Assume that if the amount of contained gas species is 10% in volume, the CO_2 droplet density is simply multiplied by weight 0.9 in our simulation since the mass of gas can be neglected by comparing to that of liquid CO_2. The range of the volume percentage of the impurity gas is from 0% to 35%. Correlation between this gas percentage and computed terminal velocity is shown in Fig. 5.

The high rising rate 20 cm/s obtained in the experiment is correspondent to the gas percentage larger than 30%. It is also found that for cases that the gas percentage is lower than 15%, the terminal velocity increases with the gas percentage linearly. It is considered that in this region, instead of the buoyancy the surface tension is considered as the dominant force. As the impurity increase further, the buoyancy becomes much more important. The droplets start to deform because the surface tension cannot balance the flow pressure due to high buoyancy. This deformation increases the drag coefficient and results in a non-linear behavior of the rising rate. The video captured in the experiment[1] indeed shows large deformation of the droplet. Therefore, we can presumably conclude that to achieve the 20 cm/s rising rate, the contained gas percentage is in the non-linear region and must be over 30% in volume.

4.2 Simulation of whole rising process

The whole rising process until the disappearance of the droplet can be simulated by the analytical method described in Section 3. The dissolution is the most important factor in this stage. Since this is a long term simulation, it is not reasonable to apply LBM, which requires large memory size and long CPU time for simulation.

Some numerical simulations by using the analytical model are carried out. Fig. 6 shows the simulated rising rate and droplet size with various properties. In these simulated cases, 3 μmol/cm^2/s is used as the dissolution rate and the initial diameter of droplet is 7.0 mm. Two extreme situations are studied. One is assuming same dissolution rate to both liquid CO_2 and impurity gas but without considering compressibility of the gas. Figure 6 shows that if we do not consider gas expansion, the predicted droplet rising rate is getting smaller with the decrease of depth more quickly than that in the experiment.

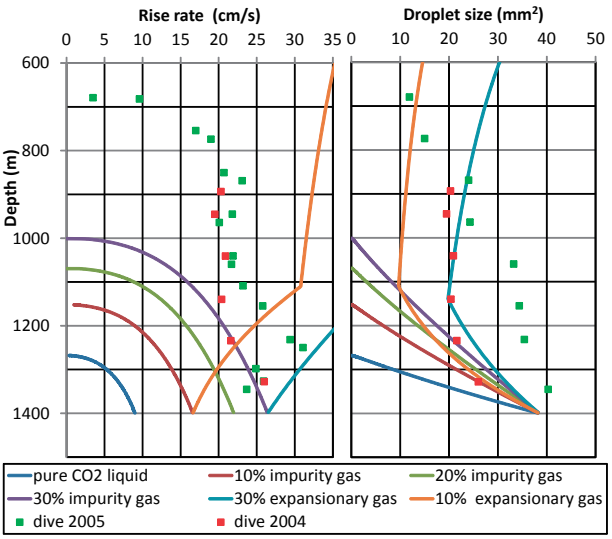

Fig. 6 Comparison of vertical change in droplet size and rise rate of CO_2 droplets between experiment and analytical model.

In the case of pure CO_2 liquid, the initial rising rate is smaller than 10 cm/s, which is similar to the above LBM result. In the case of 30 percent contained gas, the LBM predicted initial rising rate is about 20 cm/s. The present analytical method gives a result of 25 cm/s, which is close to the experimental measurement. The higher predicted terminal result than the LBM prediction is due to the neglect of droplet deformation, resulting in a smaller drag coefficient *Cd*.

In the experiment, a typical feature is that the rising rate appears to keep constant from the depth of 1400 m to 850 m. However, numerical result with the consideration of the dissolution rate cannot keep the rising rate as a constant. Another factor that should be considered is the effect of gas compressibility. Here we consider an extreme test situation. The impurity gas is undissolved in the sea water, and obeys the gas law. The reason for such treatment is that the dissolution rate of the gas is unknown. Two cases with 10 and 30 percentages in volume of expansionary gas are calculated. The gas is compressible. The volume of the droplet is then calculated by

$$V = \frac{m}{\rho_d} + V_g, \tag{18}$$

where V_g is the gas volume of the droplet that is obtained by the gas law. V_g becomes larger with the decrease of the water depth. With this expansionary gas model, the result shows obviously different curves with a winding point which indicate that the liquid CO_2 has fully dissolved and only gas bubble remained. The experimental data of rise rate exists in the area between the case of 30 percent impurity gas and 30 percent expansionary gas lines. In a real physical process the gas can also be dissolved in the seawater. This implies that such simple analytical model has the capability to simulate the experimental data when the contained gas dissolution rate to sea water is given suitably. As another future work, the accuracy of the model will be improved by using the suitable drag coefficient including the effect of deformation of droplet.

5. Conclusion

In this paper, a numerical approach is proposed to study the behavior of a natural CO_2 droplet leaked from the seafloor. Motion and deformation of the droplet at the initial stage are simulated by a LB multi-phase method to obtain the terminal velocity. The LB method is accurate and efficient for short term problem. The whole process of droplet rise is modeled by a simplified analytical method in which the CO_2 dissolution and impurity gas compressibility are considered. The proposed numerical models are applied to study of the phenomena raised in the in-situ experiment on a natural CO_2 droplet at the Okinawa Trough. From the numerical results, it is found that high rising rate measured in the experiment can be explained by the impurity gas in the initial droplet. More that 30 percent in volume of the impurity gas is required to obtain the terminal velocity measured in the experiment. From the numerical results by the analytical method, the experimental phenomena of the constant rising velocity from the depth of 1400 m to 850 m, cannot be explained by only considering the dissolution. The effect of gas expansion should be included.

Acknowledgements: This work was supported in part by World Premier International Research Center Initiative (WPI), MEXT, Japan.

References

1) K. Shitashima, Y. Maeda, Y. Koike, and T. Ohsumi, *Int. J. Greenhouse Gas Control*, **2**(1), 95 (2008).
2) P. G. Brewer, E. T. Peltzer, G. Friederich, and G. Rehder, *Environ. Sci. Technol.*, **36**(24), 5441 (2002).
3) F. Jiang and C. Hu, *Journal of Novel Carbon Resource Sciences*, **5**, 10 (2012).
4) D. d'Humières, in *Rarefied Gas Dynamics: Theory and Simulations, Progress in Astronautics and Aeronautics*, eds. by B. D. Shizgal and D. P. Weaver, Vol. 159, American Institute of Aeronautics and Astronautics, Washington, DC, p. 450 (1992).
5) A. K. Gunstensen, D. H. Rothman, S. Zaleski, and G. Zanetti, *Physical Review A*, **43**, 4320 (1991).
6) B. Ahrenholz, Ph. D. Thesis, Technische Universität Braunschweig, Braunschweig, Germany (2009).
7) J. Tölke, S. Freudiger, and M. Krafczyk, *Computers & Fluids*, **35**(8-9), 820 (2006).
8) P. Lallemand, L. Luo, *Physical Review E*, **61**(6), 6546 (2000).
9) J. Tölke, M. Krafczyk, M. Schulz, and E. Rank, *Philosophical Transactions: Mathematical, Physical and Engineering Sciences*, **360**(1792), 535 (2002).
10) D. Kehrwald, Ph. D. Thesis, University of Kaiserslautern, Kaiserslautern, Germany (2003).
11) M. Ozaki, J. Minamiura, Y. Kitajima, S. Mizokami, K. Takeuchi, K. Hatakenaka, *Journal of Marine Science and Technology*, **6**(2), 51 (2001).